

Stability, geometry and electronic properties of BH_n ($n = 0$ to 3) radicals on the $Si\{0\ 0\ 1\}3$ 1:H surface from first-principles

Fang, C. M.; Mohammadi, V.; Nihtianov, S.; Sluiter, M. H.F.

DOI

[10.1088/1361-648X/ab6e43](https://doi.org/10.1088/1361-648X/ab6e43)

Publication date

2020

Document Version

Final published version

Published in

Journal of Physics Condensed Matter

Citation (APA)

Fang, C. M., Mohammadi, V., Nihtianov, S., & Sluiter, M. H. F. (2020). Stability, geometry and electronic properties of BH_n ($n = 0$ to 3) radicals on the $Si\{0\ 0\ 1\}3$ 1:H surface from first-principles. *Journal of Physics Condensed Matter*, 32(23), Article 235201. <https://doi.org/10.1088/1361-648X/ab6e43>

Important note

To cite this publication, please use the final published version (if applicable). Please check the document version above.

Copyright

Other than for strictly personal use, it is not permitted to download, forward or distribute the text or part of it, without the consent of the author(s) and/or copyright holder(s), unless the work is under an open content license such as Creative Commons.

Takedown policy

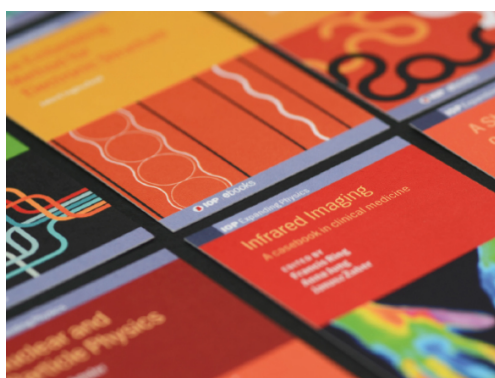
Please contact us and provide details if you believe this document breaches copyrights. We will remove access to the work immediately and investigate your claim.

PAPER • OPEN ACCESS

Stability, geometry and electronic properties of BH_n ($n = 0$ to 3) radicals on the $\text{Si}\{001\}3 \times 1\text{:H}$ surface from first-principles

To cite this article: C M Fang *et al* 2020 *J. Phys.: Condens. Matter* **32** 235201

View the [article online](#) for updates and enhancements.



IOP | ebooksTM

Bringing together innovative digital publishing with leading authors from the global scientific community.

Start exploring the collection—download the first chapter of every title for free.

Stability, geometry and electronic properties of BH_n ($n = 0$ to 3) radicals on the $\text{Si}\{001\}3 \times 1:\text{H}$ surface from first-principles

C M Fang¹, V Mohammadi², S Nihtianov² and M H F Sluiter³

¹ BCAST, Brunel University London, Kingston Lane, Uxbridge, Middlesex, UB8 2AD, United Kingdom

² Electronic Instrumentation Lab, Faculty of Electrical Engineering, Mathematics and Computer Science, TU Delft, Mekelweg 4, 2628 CD Delft, The Netherlands

³ Department of Materials Science and Engineering, TU Delft, Mekelweg 2, 2628 CD Delft, The Netherlands

E-mail: Changming.Fang@brunel.ac.uk

Received 5 October 2019, revised 20 December 2019

Accepted for publication 21 January 2020


Published 10 March 2020



Abstract

A new generation of radiation detectors relies on the crystalline Si and amorphous B (c-Si/a-B) junctions that are prepared through chemical vapor deposition of diborane (B_2H_6) on Si at low temperature ($\sim 400^\circ\text{C}$). The Si wafer surface is dominated by the $\text{Si}\{001\}3 \times 1$ domains that consist of two different Si species at low temperature. Here we investigate the geometry, stability and electronic properties of the hydrogen passivated $\text{Si}\{001\}3 \times 1$ surfaces with deposited BH_n ($n = 0$ to 3) radicals using parameter-free first-principles approaches. *Ab initio* molecular dynamics simulations using the density functional theory (DFT) including van der Waals interaction reveal that in the *initial* stage the BH_3 molecules/radicals deposit on the Si(-H), forming $(-\text{Si})\text{BH}_4$ radicals which then decompose into $(-\text{Si})\text{BH}_2$ with release of H_2 molecules. Structural optimizations provide strong local relaxation and reconstructions at the deposited Si surface. Electronic structure calculations reveal the formation of various defect states in the forbidden gap. This indicates limitations of the presently used rigid electron-counting and band-filling models. The attained information enhances our understanding of the *initial* stage of the PureB process and the electric properties of the products.

Keywords: depositions and chemical reaction, BH_n radicals, $\text{Si}(001)$ surface, *ab initio* molecular dynamics, electronic properties


 Supplementary material for this article is available [online](#)

(Some figures may appear in colour only in the online journal)

1. Introduction

The developments of new technologies, such as micro-photolithography and nanoelectronics demand high-performance radiation detectors for e.g. NUV (near ultra-violet) or

VUV (vacuum ultra-violet) photons [1–3]. Si-based photodiodes are good candidates for the above mentioned applications, due to their advantages, such as low-cost and well-developed techniques [1–4]. Meanwhile, they have an extremely small penetration depth of the NUV/VUV radiations and therefore, require the depletion zone of the photodiode to be very close to the device surface. Such unusual device has been realized recently by the PureB process which involves pure amorphous boron (a-B) deposition on crystalline Si (c-Si) to produce

 Original content from this work may be used under the terms of the [Creative Commons Attribution 4.0 licence](#). Any further distribution of this work must maintain attribution to the author(s) and the title of the work, journal citation and DOI.

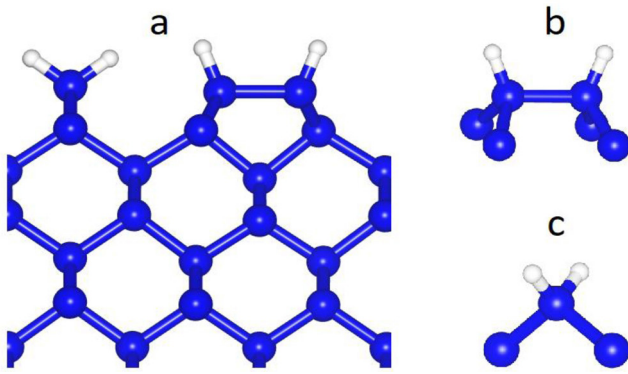


Figure 1. Schematic structure of the H passivated Si{001}3 × 1 surface (a) and the coordination of the related Si1 (b) and Si2 (c).

c-Si/a-B junctions by means of chemical vapor deposition (CVD) of diborane (B_2H_6) [1–7]. The process also produces controllable thicknesses of the boron layers. A rapid smooth growth of a boron monolayer on Si surfaces has been realized at low temperature of about 400 °C.

The low-temperature PureB process produced c-Si/a-B (crystalline silicon/amorphous B) junctions contain little B–Si mixture [7, 8]. In this temperature range, the widely used Si{001} wafer is reconstructed into Si{001}3 × 1 domains, in which there are two distinct type Si species, Si1 and Si2 [9, 10]. This surface can be hydrogen passivated in an H atmosphere [9, 10, 15]. After H-passivation Si1 is coordinated with three Si (two from the subsurface and one at the surface) and one H on top (figure 1(b)), whereas Si2 has two Si neighbors from the subsurface and two H on top, as shown in figure 1(c). Experiments also provided that even very thin depositions (~0.2 atomic layers) change the electrical properties of the system [3–5, 7]. Therefore, knowledge about the electronic properties of the dilute BH_n ($n = 0$ to 3) radicals on the Si surfaces is vital for understanding the underlying physics.

Up to now, experimentalists have focused on the structure of the diborane molecule [9] and its decomposition reactions [1–5, 11–15]. First-principles approaches have been applied to investigate the geometries of pure Si surfaces [9, 10, 16], the Si surfaces with hydrogen-termination [10], B doping in Si [17–19], and B on the Si surfaces [19–21]. We investigated deposition of BH_n ($n = 0$ to 3) radicals on the Si{001}2 × 1:H surface [22] which is stable at high temperature (~640 °C [15]). Here we further investigate the deposition of the BH_n ($n = 0$ to 3) radicals on the Si{001}3 × 1:H surface which has high stability at low temperature [15]. The calculations produce details of the optimized structures and related energetics for BH_n radicals on the Si{001}3 × 1:H surface and provide a static picture about the *initial* stage of PureB process. *Ab initio* molecular dynamics (AIMD) technique was also employed to model the processes of BH_3 depositing on the Si{001}3 × 1:H surfaces. The attained information here sheds some light on the related reactions and the electronic properties of the products of the PureB process.

2. Computational details

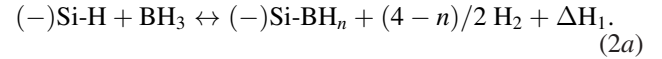
2.1. Reactions and formation energetics on the H passivated Si{001}3 × 1 surface

Experiments revealed that on Si surfaces at elevated temperature, one B_2H_6 molecule decomposes into two boron trihydride molecules [1–3, 15, 22]:

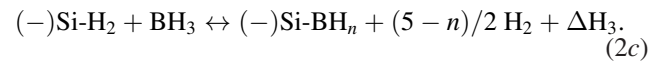
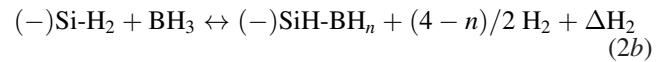


Then the depositions of dilute BH_n radicals occur from the BH_3 molecules on the Si surfaces in the following reactions:

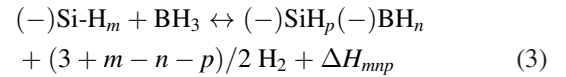
For the reaction on Si1 which has one H on top (figure 1(b)),



There are two possibilities for the reaction on Si2 which has two H on top (figure 1(c))

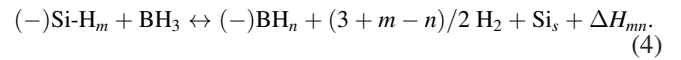


The above reactions can be summarized as



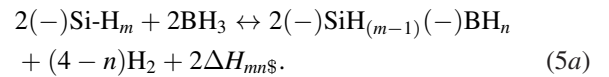
where $m = 1$ or 2; $n = 0$ to 3, $p = 0$ or 1.

For the replacement of one SiH_m ($m = 1, 2$) by one BH_n at the Si surface,

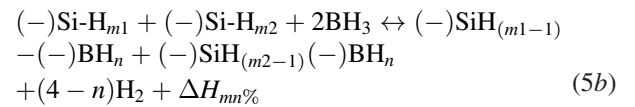


Here Si_s represents a Si atom that belongs to the solid substrate.

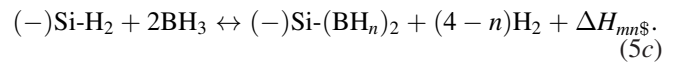
The reaction of two BH_n radicals on two Si surface atoms of the same type is:



For the reaction of two BH_n radicals simultaneously on one Si1 and on one Si2 surface atom,



and the reaction of two BH_n radicals on one Si2 of the surface is:



Here, ΔH represents the formation enthalpy of reactions. At temperature $T = 0$ K, and pressure $P = 0$ Pa, the corresponding enthalpies, such as that of the silicon surfaces systems $H(-SiH_m)$, here $m = 1$ for Si1 for $m = 2$ for Si2, of the

isolated BH_3 molecule $H(\text{BH}_3)$, as well as those of the products, e.g. $H(\text{H}_2)$ for an isolated H_2 molecule, $H(\text{Si}-\text{BH}_n)$ for $(-)\text{Si}-\text{BH}_n$, are equal to the corresponding total enthalpies which can be obtained from our first-principles calculations. The formation energy is equal to the formation enthalpy, $\Delta E = \Delta H$, when contributions from zero-point vibrations are ignored. A negative value of ΔH indicates that the left to right direction of the reaction is energetically favoured (exothermic).

2.2. $\text{Si}\{001\}3 \times 1$ surface and its 2D cells

Si has a diamond structure with the (cubic) lattice parameter of 5.431 Å. The Si atoms are in a tetrahedral coordination [23]. A cleavage perpendicular to the [001] axis produces two $\text{Si}\{001\}$ surfaces. The Si surface atoms have only two nearest neighbours from the subsurface layer. This pristine $\text{Si}\{001\}$ surface is unstable at elevated temperature. At temperature around 400 °C, it reconstructs into the 3×1 domain with two inequivalent Si surface sites: Si1 with three neighbours and Si2 with two Si neighbours [15]. This reconstructed surface can be stabilized by hydrogen passivation [15]. After H passivation each Si1 absorbs one H and each Si2 is terminated by two H. In this way the tetrahedral coordination is restored for the surface Si atoms (figure 1). The unit cells for the $\text{Si}\{001\}3 \times 1:\text{H}$ domains are orthorhombic with the surface plane lattice parameters: $a = \sqrt{2} a_0$, $b = 3 \sqrt{2/2} a_0$ (a_0 is the lattice parameter of bulk Si). We utilize a supercell to investigate the $\text{Si}\{001\}3 \times 1:\text{H}$ reconstructed surface where the thickness of the slab is along the c -axis, and where every Si layer contains 6 Si atoms. The slab is 16 atomic layers (AL) thick to assure that bulk-like properties are attained in the middle of the slab. The thickness of the vacuum region is at least 12 Å to avoid inter-slab interactions. In this way we employed an orthorhombic supercell with $a = 7.77$ Å, $b = 11.65$ Å and $c = 34.96$ Å which contains 96 Si atoms in the substrate with consideration of the localized nature of influence of the deposited BH_n at the Si substrate (see section 3.4). We employed these supercells to balance the reliability and accuracy of calculations and the computational requirements.

For the deposition of an isolated BH_n on the $\text{Si}\{001\}3 \times 1:\text{H}$ surface, we put one BH_n radical on either a Si1 or a Si2 atom. Furthermore, we also consider the cases with two BH_n in one surface cell in order to understand the possibilities of BH_n interaction with each other on the surface.

2.3. The computational details

Our approach is based on the first-principles density-functional theory (DFT) [24, 25]. The first-principles code VASP (Vienna *ab initio* simulation program) [26, 27] was employed. This code uses periodic boundary conditions. We use the projector augmented-wave (PAW) method within [28, 29] the generalized gradient approximation (GGA) as formulated by Perdew, Burke and Ernzerhoff (PBE) [30]. The electronic configurations for the present calculations are H $1s^1 2p^0$, B [He] $2s^2 2p^1$ and Si [Ne] $3s^2 3p^1$.

For all the calculations, we employ $E_{\text{cut}} = 550.0$ eV for the plane wave expansion of the valence electrons and $E_{\text{aug}} = 700.0$ eV for the augmented waves. The present settings are significantly higher than the corresponding default cut-off energy values in the potentials (the default energies, $E_{\text{NMAX}} = 400.0$ eV for H, 322.069 eV for Si and 318.64 eV for B, respectively). Test calculations confirmed good convergence of the stress tensor and the atomic force for the strongly covalent solids using the present settings. We used the same settings for all calculations. This provides a systematic cancellation of errors. Calculations included spin-polarization but converged to spin-degenerate states for most calculations. Although in principle all the valence electrons belong to the whole crystal rather than to the individual atoms/ions, the calculated plane waves/electron density can be projected onto atomic orbitals to obtain the atom decomposed local charges and partial and total density of states (DOS). The electronic wave functions were sampled on $9 \times 6 \times 1$ grid (20k-points) in the Brillouin zone (BZ) of crystals using Γ -centred k -meshes for all supercells [31]. Tests of k -meshes and cut-off energies showed energy convergence within 1 meV/atom.

The *ab initio* MD simulation utilizes the finite-temperature density functional theory of the one-electron states, the exact energy minimization and calculation of the exact Hellmann–Feynman forces after each MD step using the preconditioned conjugate techniques, and the Nosé dynamics for generating a canonical NVT ensemble [26]. For AIMD simulations, only the Γ -point (0,0,0) was used and smaller cut-off energies ($E_{\text{nMAX}} = 320$ eV) were employed.

3. Results and discussions

We first study the reactants, the isolated H_2 and BH_3 molecules, as well as Si bulk and the $\text{Si}\{001\}3 \times 1:\text{H}$ slab. The calculated H–H bond length for H_2 is 0.748 Å, in good agreement with the experimental value (0.7414 Å) [32]. An isolated BH_3 molecule has a planar structure with a calculated B–H bond-length of 0.965 Å (experimental value: 0.924 Å) [33]. Furthermore, our structural optimization for the slab of the passivated $\text{Si}\{001\}3 \times 1:\text{H}$ surfaces, the square unit cell in plane has a length of 5.494 Å. This value is slightly larger than that of experimental values of the bulk silicon (5.431 Å) [23]. Such slight overestimations of the bond-lengths/lattice parameters are not unusual for the DFT-GGA approximation [34].

3.1. Clean and H passivated $\text{Si}\{001\}3 \times 1$ surfaces

The bond lengths of hydrogen-passivated Si1 are 2.39 Å ($2\times$) and 2.44 Å for Si–Si and 1.49 Å for Si–H. The bond lengths of the H passivated Si2 are 2.38 Å ($2\times$) for Si–Si and 1.49 Å ($2\times$) for Si–H (figure 1). The calculated Si–H bond-lengths agree well with the experimental values (1.49 Å) [10, 15]. The good agreement between the theoretical calculations and experimental values suggest that the present accuracy settings are adequate for making predictions concerning borane

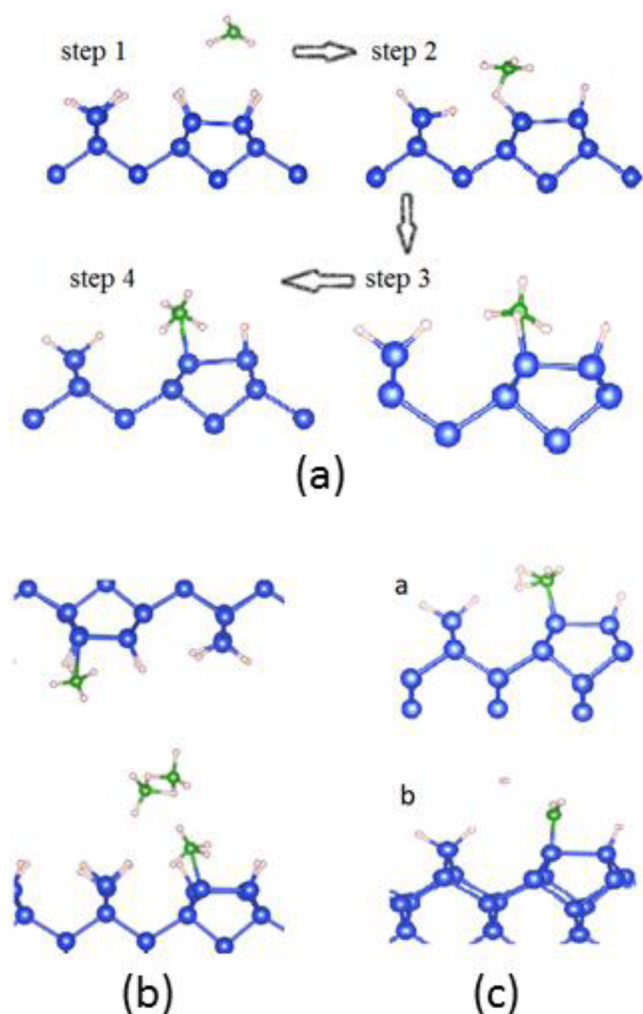


Figure 2. The schematic pictures for one BH_3 molecule deposition to form one $-\text{SiBH}_4$ configuration on the H passivated $\text{Si}\{001\}3 \times 1:H$ surface from AIMD simulations including van der Waals interaction (a). A snap shoot the simulated system containing two $-\text{SiBH}_4$ configurations with Si–H–B bonding and one $(\text{BH}_3-\text{BH}_3)$ during the MD simulations (b), and a medium configuration of one $-\text{SiBH}_4$ configuration c_a) and its final state which contains a H_2 molecule and $-\text{SiBH}_2$ configuration during its transition, c_b).

molecules, silicon surfaces with/without hydrogen termination, as well as Pure B on and in the Si surfaces.

We analyzed the charges at atomic sites using Bader's charge model [35–37]. The obtained atomic charges for the $\text{Si}\{001\}3 \times 1:H$ surface are found to be $(-)(\text{Si}1)^{+0.57}\text{H}^{-0.60}$ and $(-)(\text{Si}2)^{+1.18}(\text{H}^{-0.62})_2$, respectively. Such charge transfers from Si to H are in line with the electronegativity difference between Si (1.9 in Pauling scale) and H (2.2).

There are two possible sites that feature Si dangling bonds on the surface that get saturated by H: One by desorbing H on Si1 and another two on Si2. Our first-principles calculations showed that de-absorption of one H at the $\text{Si}\{001\}3 \times 1:H$ surface costs 1.57 eV for an H on Si1 and 1.72 eV for an H on Si2 site, respectively. Such moderate enthalpy difference (0.15 eV) indicates that at elevated temperature and in an H-poor atmosphere, H desorption may occur at both Si1 and

Si2 though its occurrence at Si1 is slightly favored at elevated temperature.

3.2. AIMD simulations for BH_3 deposition on $\text{Si}\{001\}3 \times 1:H$

To get some insight into the deposition of BH_3 molecules on the $\text{Si}\{001\}3 \times 1:H$ surface, we performed AIMD simulations. We added four BH_3 molecules into the vacuum between the Si surfaces. The simulation temperature was selected as 673 K (400 °C). van der Waals interaction correction [38, 39] was included as it has been shown that the standard DFT method without van der Waals interaction correction describe improperly the interaction between molecules themselves and between molecules and substrate [39, 40]. The simulations lasted over 10 ps (7000 steps at 1.5 fs/step). The processes and the reactions are schematically shown in figure 2.

During the MD processes we observed the movements of the BH_3 molecules on the H passivated $\text{Si}\{001\}3 \times 1$ surfaces, the formation of a B_2H_6 molecule from two BH_3 molecules in the space, and the formation of $(-)\text{SiBH}_4$ molecules on the surface (figure 2). The deposition of BH_3 molecules occurs on the Si1 site during our simulation. Here we address this surface reaction in more detail. After a few picoseconds (ps), one BH_3 molecule approaches an H which is bonded to Si1. At this moment, the B in the BH_3 was having two extra neighbors: one H and the related Si. Finally, the BH_3 becomes deposited on the Si surface with four H bonded to it to form $(-)\text{SiBH}_4$ configuration. This configuration persists in the following 10 ps (about 7000 steps) in the simulations. Further MD simulations reveal the decomposition of the $(-)\text{SiBH}_4$ configurations. As shown in figure 2(c), two H atoms in the $(-)\text{SiBH}_4$ radical approach to each other and bond to each other gradually, and finally the formed H_2 molecule moves away from the radical. The final products are one H_2 molecule and the remaining $(-)\text{SiBH}_2$ radical.

3.3. Isolated BH_n ($n = 0$ to 3) radicals on and at the $\text{Si}(100)3 \times 1:H$ surface

Total energy calculations for the optimized structures showed that an isolated B on the $\text{Si}\{001\}3 \times 1:H$ surface has high formation enthalpy (about +4.3 eV) (see the supplementary materials, figure SM-1 (stacks.iop.org/JPhysCM/32/235201/mmedia)). This value is close to that (+4.2 eV) for one B on Si in the $\text{Si}\{001\}2 \times 1:H$ surface [22]. This indicates little possibility to form dilute bare B on the Si surfaces in a H_2 -rich environment according to the definition in the equations (2)–(5). Meanwhile, H passivation of the isolated B increases the stability. The formation of one BH deposition on the surface Si costs about 2.3 eV. Figure 3 shows that the formations enthalpies of an isolated BH_2 or BH_3 on the Si surface are positive ranging from -0.15 to -0.36 eV (figures 3(a)–(d)). This suggests that both dilute BH_2 and BH_3 can be formed on the $\text{Si}\{001\}3 \times 1:H$ surface. The stability of BH_2 radicals on this surface was also reflected in the molecular dynamics simulations (figure 2(c)). This corresponds to the

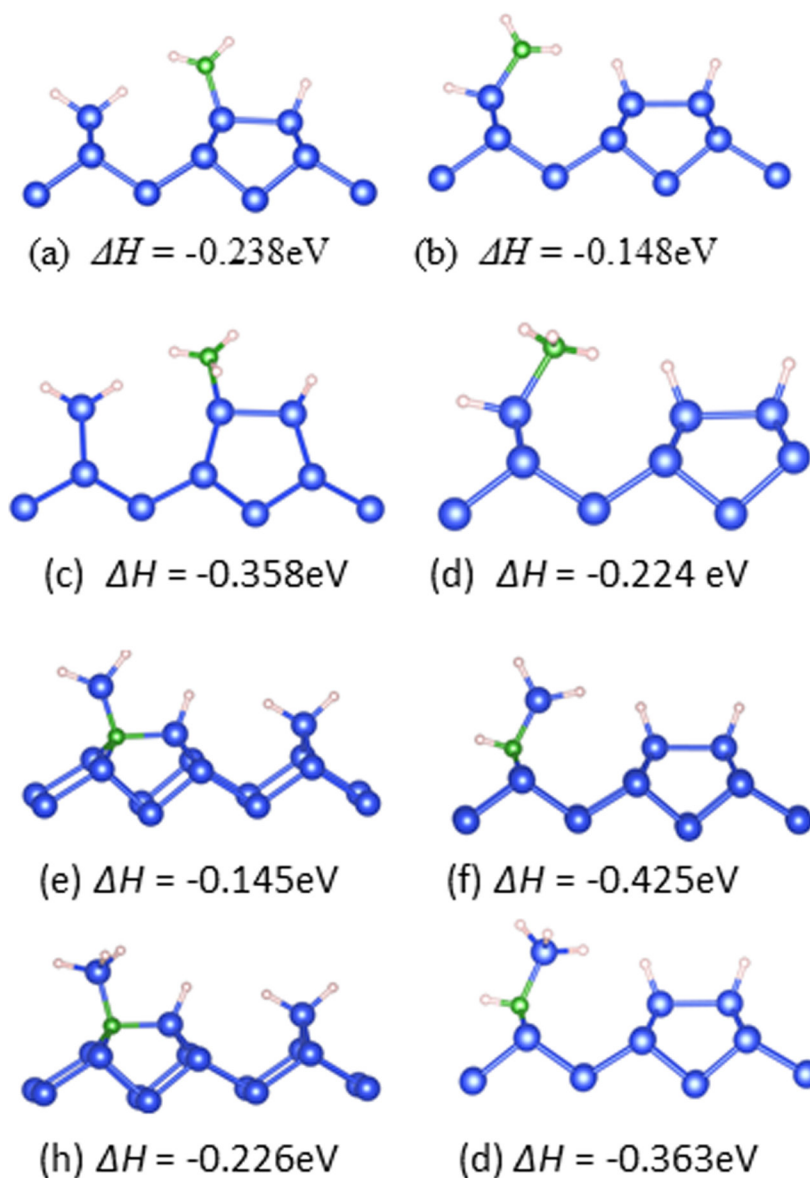


Figure 3. Schematic structures and the related formation enthalpies of the exchange between Si on/at the surface and B in BH_n ($n = 2, 3$) radicals at and on $\text{Si}\{001\}3 \times 1:\text{H}$ surfaces: (a) BH_2 on Si1, (b) BH_2 on Si2, (c) BH_3 on Si1 and (d) BH_3 on Si2; and (e) SiH_2 on B1-at-surface, (f) SiH_2 on B2-at-surface; (g) SiH_3 on B1-at-surface and (h) SiH_3 on B2 at surface. The blue, green and white spheres represent Si, B and H, respectively. The local bonding is summarized in table SM-1.

preferred coordination numbers (3 or 4) for B (table SM-1). The structural analysis also showed that deposition of isolated BH_n radicals on $\text{Si}\{001\}3 \times 1:\text{H}$ surfaces cause local structural relaxations. The important chemical bonds and charges at the surface atoms/ions are shown in table SM-1.

Next we discuss the exchange of the B in the deposited BH_n radicals and the adjacent Si, an important step for B depositing on Si. The results are shown in figures 3(e)–(h) for the configurations of high stability.

The calculations showed that the $(-)\text{B}-\text{Si}$ and $(\text{B})-\text{SiH}$ depositions are not favored (figure SM-2), meanwhile, formations of $(-)\text{B}-\text{SiH}_2$ and $(-)\text{B}-\text{SiH}_3$ radicals at both Si1 and Si2 sites are favored with formation enthalpies ranging from -0.145 to -0.363 eV as shown in table SM-1. Figures 3(e)–(h) shows the schematic structures of the stable configurations with the exchange of B in the deposited BH_n

radical with the surface Si it attached to form $\text{B}-\text{SiH}_n$ ($n = 2, 3$). The unstable configurations with the exchange of B in the deposited BH_n radical with the surface Si it attached to form $\text{B}-\text{SiH}_n$ ($n = 0, 1$) are schematically shown in figure SM-2. The corresponding bond-lengths and charges at the atomic sites for all structures are in table SM-1. As shown in figures 3(e)–(h), the frames of the optimized structures of the BH_n ($n = 2, 3$) radicals on the Si atoms/ions remain while relaxation occurs.

In table SM-1, details of the local chemical bonds are given. From $n = 1$ to $n = 3$, the $\text{B}-\text{Si}$ bond-length notably increases while the $\text{B}-\text{H}$ bond-length increases only moderately. Charge analysis shows an interesting trend. The charges at H are almost constant: about $-0.63e$ for H on Si and about $-0.59e$ for the H at B (table SM-1). This corresponds to the slightly more electronegative nature of B than Si. Structural optimizations

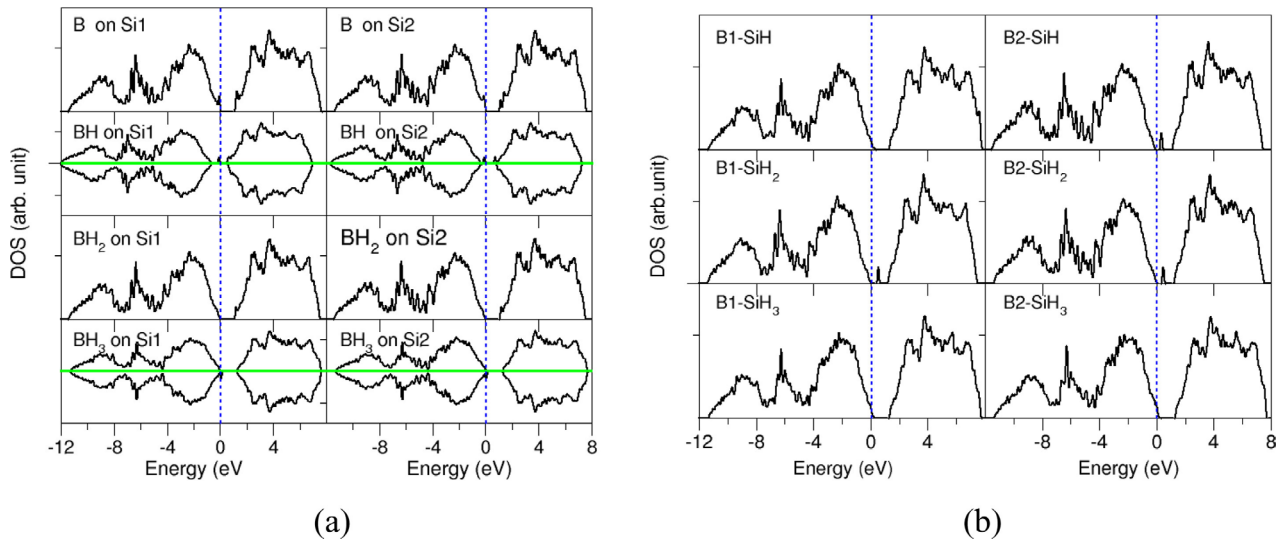


Figure 4. Total density of states for the $\text{Si}\{001\}3 \times 1:\text{H}$ surface with one BH_n radical on the Si1 or Si2 atom/ion in corresponding to figure 3(a); for the $\text{Si}\{001\}3 \times 1:\text{H}$ surface with exchanged Si at the surface and B from the BH_n radicals (figure 3) (b), respectively.

for the B/Si exchange systems (figures 3(e)–(h)) showed that all the B atoms are four fold coordinated. In fact there is no reconstruction for the B atoms/ions now at the surfaces. All the B atoms/ions in the Si1 site are in four-fold coordinated by Si and all the B at the Si2 sites are coordinated by 3 Si and one H. The local structure after the Si/B exchange changes little, displaying only minor local relaxation.

Formation of $(-)\text{BH}_n$ ($n = 0$ to 3) radicals at the $\text{Si}(100)3 \times 1:\text{H}$ is also investigated. As shown in figure SM-2 and table SM-1, when a BH_n molecule replaces a Si–H on the $\text{Si}\{001\}3 \times 1:\text{H}$ surface, the formation enthalpies using equation (4) are moderately high (about +2.0 eV). Therefore, one expects low possibility of formation of such configurations. However, these configurations may form at special conditions such as under ion attack and at elevated temperature in an H-poor atmosphere, etc. Therefore, we also include their electronic properties in table SM-1. Overall from the calculations, one can conclude that the high stability of a BH_3 on one of the two Si sites indicates a high probability of direct BH_3 deposition at the *initial* stage and those BH_3 originate from the decomposition of diborane molecules.

We performed electronic structure calculations for the isolated BH_n ($n = 0$ to 3) deposited on the $\text{Si}\{001\}3 \times 1:\text{H}$ surfaces. The obtained electronic densities of states (DOS) are shown in figure 4.

Figure 4 shows that the frames of all the curves are similar to that of pure $\text{Si}\{001\}3 \times 1:\text{H}$ surface. However there are defect states in the forbidden gap. Clearly these defect states are dispersion-less and very localized. Therefore, we analyzed the energy positions of the defect/impurity states in the band gaps of the surfaces and summarized the results in table SM-1. The notable defects are the most stable B– SiH_2 at the Si1 and Si2 which have unoccupied defect states at about 0.5 eV above the valence band maxima (VBM). Naturally these defect states have strong influence on the electronic properties of the system even at such low coverage. These defect states could

not be predicted by the simple rigid electron-counting and band-filling model [3–5].

3.4. Two BH_n ($n = 0$ to 3) radicals on the $\text{Si}(100)3 \times 1:\text{H}$ surface

The two different surface Si species (figure 1) indicates more possibilities to deposit two BH_n on the $\text{Si}\{001\}3 \times 1$ surface. Analysis showed that there are five ways to deposit two BH_n radicals on the $\text{Si}\{001\}3 \times 1:\text{H}$ surface: (1) on a bridging Si1 pair; (2) two separated Si1; (3) one Si1 and one Si2; (4) on one Si2 and (5) on two Si2. In next sections, we focus the optimized structure and formation enthalpies of the above mentioned systems in two parts. The formation enthalpies were calculated from the cohesive energies of the configurations and the related Si surfaces and boranes according to equations (5a)–(5c).

First we address the two B atoms or BH radical on the surface with the optimized structures and related formation enthalpies in figure SM-3. For two B deposited on two separated Si1, the formation enthalpy is about +4.24 eV/B, which is close to that of the dilute case (+4.20 eV, table SM-1). In fact the calculated B–Si bond lengths and the charge transfers in the two cases are also similar (tables SM-1 and SM-2). The present results indicate that the influence of the BH_n deposition at the Si surfaces is highly localized.

Meanwhile, when two B were put on a bridging Si–Si pair, structural reconstruction occurs. The two B atoms also form a B–B pair. As a consequence, the formation enthalpy is strongly reduced to about +2.5 eV/B (figure SM-3(d)) from about +4.24 eV/B (figure SM-3(a)). When two B atoms were put at a Si1 and at a Si2, interesting reconstruction occurs. The B on Si1 behaves normally as the dilute case while for the B on Si2, the H originally on the Si2 moves to the top of B, forming a Si–B–H chain. The calculated formation enthalpy is also reduced to about +3.5 eV mainly due to the

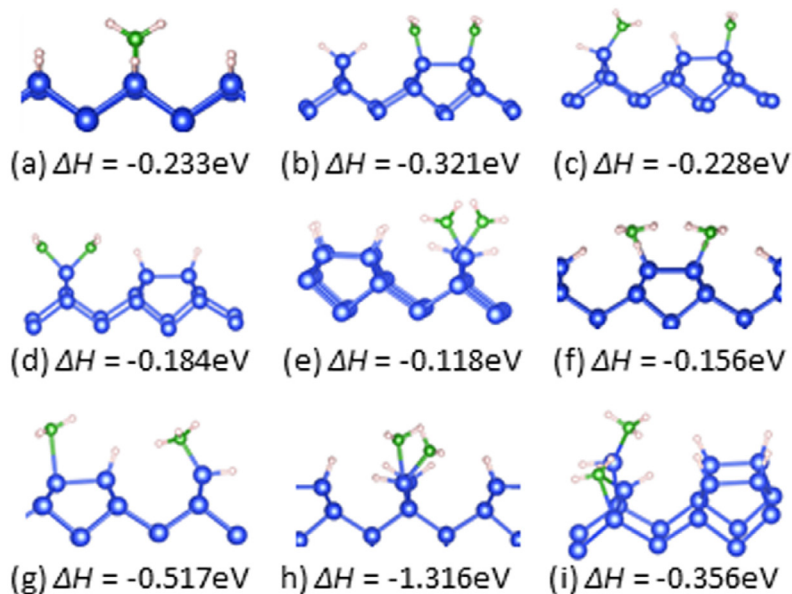


Figure 5. Schematic structures and the related formation enthalpies of two BH_n ($n = 2, 3$) radicals on $\text{Si}\{001\}3 \times 1:\text{H}$ surfaces. (a) two BH_2 on two bridging $\text{Si}1$; (b) two BH_2 on two separated $\text{Si}1$ sites; (c) two BH_2 on one $\text{Si}1$ and one $\text{Si}2$; (d) two BH_2 on one $\text{Si}2$; (e) two BH_2 on two separated $\text{Si}2$; (f) two BH_3 on two bridging $\text{Si}1$; (g) two BH_3 on two separated $\text{Si}1$; (h) two BH_3 on one $\text{Si}2$; and (i) two BH_3 on two separated $\text{Si}2$. The formation enthalpies were obtained from equations (2), (3) and (5). The blue spheres represent Si, green for B and small white for H.

reconstruction of the B on $\text{Si}2$. Another notable case is the two B on one $\text{Si}2$ atom (figure SM-3(d)). The structural relaxation also causes a B–B bond. This structure has also quite low formation enthalpy (about $+2.8\text{eV/B}$). Figure SM-3 showed a structural reconstruction of two B at two $\text{Si}2$. The B atoms move inwards to form a one-dimensional (1D) B–Si–B–Si chain. Furthermore, the H atoms on $\text{Si}2$ also move on the B tops.

Comparison of figures SM-3(a) and SM-3(b) showed that the formation of B–B bond strongly reduces the formation enthalpy of the system. Figure SM-3 shows the optimized structures for 2BH radicals on the $\text{Si}\{001\}3 \times 1:\text{H}$ surface. When the two BH radicals were put at two separated $\text{Si}1$, the local structure relaxes similar to that of the dilute case, though the formation enthalpy is reduced to about $+1.4\text{eV/BH}$. Similar to the case of two B on a $\text{Si}1$ – $\text{Si}1$ pair, when two BH radicals were put on a $\text{Si}1$ – $\text{Si}1$ pair, there is also a B–B bond formed. The formation enthalpy is rather lower ($+0.94\text{eV/BH}$) as shown in figure SM-3 and table SM-2. When two BH radicals were put on one $\text{Si}1$ and on one $\text{Si}2$ at the same time, structural reconstruction occurs. The B on $\text{Si}1$ moves towards $\text{Si}1$. One H on $\text{Si}2$ also moves to the top of the B on $\text{Si}2$. As a result, both B atoms are three-fold coordinated: B1 has two Si neighbors and one H on top while B2 has one $\text{Si}2$ neighbor and two H on top. The formation enthalpy is also very low ($+0.65\text{eV/B}$). The cases of two BH on two $\text{Si}2$ are rather simple: one B–B bond for two BH on one $\text{Si}2$, meanwhile, only relaxation occurs for the case two BH on two separated $\text{Si}2$ with the formation enthalpies of $+1.3$ to $+1.7\text{eV/BH}$.

In summary, for the cases of BH radicals on Si, the calculations showed that B–B formation (figure SM-3) or one B connecting to two Si reduces the formation enthalpies notably. Such low positive formation enthalpies indicate possibilities

of the formation of these configurations at elevated temperature and H-poor conditions.

Here we discuss two BH_n ($n = 2, 3$) radicals the Si atoms/ions in a unit cell of the $\text{Si}\{001\}3 \times 1:\text{H}$ surface. The optimized structures are shown in figure 5 and in Table SM-2.

Due to the fact that the coordination number of B for the BH_2 radicals deposited on the Si is three, one expects no significant structural relaxation to occur. That is true as shown in figures SM-3(a) to (e). Each B is coordinated to one Si with B–Si bond lengths of about 2.0Å and to two H (B–H: 1.19Å). The formation enthalpies are also quite close in the range of -0.15 to -0.36eV which also close to that of isolated BH_2 deposition (table SM-2). Structural reconstruction occurs for almost all the cases of two BH_3 molecules. The only exception is the case that two BH_3 were deposited on a $\text{Si}1$ – $\text{Si}1$ pair whereby only structural relaxation occurs and each B is connected to one Si and three H as shown in table SM-2. When the two BH_3 were put on two separated $\text{Si}1$, one B (B1) still has a coordination similar to that of a dilute case with one Si and three H neighbors, the other B (B2) moves to a middle position and connected to two Si and therefore, it has five neighbors. Such structural reconstruction reduces its formation enthalpy to -0.52eV (figure 5). Structural optimizations for two BH_3 on one $\text{Si}1$ and $\text{Si}2$ showed that the BH_3 molecule on $\text{Si}1$ tends to move away from the surface.

We repeated this configuration with various starting conditions but in each case the same qualitative behavior was observed.

When two BH_3 molecules were set on one $\text{Si}2$, structural reconstruction produced five-coordinated B atoms/ions with one B–B bond. That is, each B has one Si, one B and three H neighbors. This type of bonding is quite unusual, but such reconstruction produced a very stable surface structure

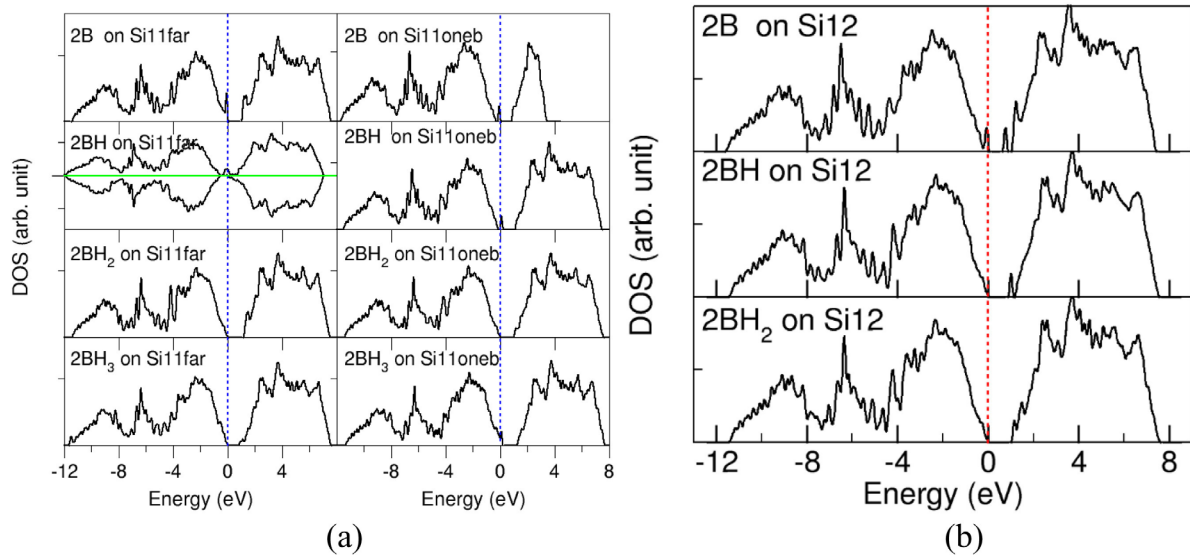


Figure 6. Calculated electronic structures for the $\text{Si}\{001\}3 \times 1:\text{H}$ surfaces with two BH_n ($n = 0$ to 3) radicals on with: (a) the total DOS curves for two BH_n on two surface Si1 atoms/ions; (b) the total DOS curves for two BH_n on one surface Si1 and one Si2 atoms/ions; (c) the total DOS curves for two BH_n on two surface Si2 atoms/ions. The sign Si22far means two separated Si atoms; Si22one means at two bridging Si1 atoms; Si22one means at one Si2 atom/ion.

as shown in table SM-2. Putting two BH_3 on two separated Si2 resulted in structural reconstruction as well. One of the B is connected to two Si, meanwhile, the other one is in four coordination.

The calculations also showed possibilities of BH_n clustering on the surface. Overall, the formation enthalpies of two BH_n radicals on the surface are equal to or lower than that of corresponding dilute cases. The calculations showed that formation of B–B bonds or B connected to two Si atoms on the surface strongly reduces formation enthalpies. That indicates a high probability of B clustering.

As shown in figure 6, the frames of the electronic structures of all the configurations are similar to that of the pure $\text{Si}\{001\}3 \times 1:\text{H}$. That is understandable since our simulated systems contain only dilute BH_n radicals in accordance with the fact that at the *initial* stage the deposition of BH_n radicals occurs locally. The structural optimizations showed a) for dilute cases with BH_n on Si, only local relaxation occurs and the coordination number of B increases with increasing n of the BH_n radical (table SM-1 and figure 3). For $n = 0$ and 2, there are no defect states at the forbidden gaps. Meanwhile, there are defect states exits for systems containing a BH radical on it. This is more or less corresponding to the rigid electron accounting and band-filling model. However, for $n = 3$ there are no defect states in the forbidden gaps, as shown in figure 4 and table SM-1. This violates the rigid electron accounting model. Another interesting issue is the high stability of the systems with B/Si exchanges to form B– SiH_n configurations. All B in these configurations are four-fold coordinated. Meanwhile their electronic properties are rather complex: half of them have defect states in the energy gaps meanwhile the other half have no defect states (table SM-1).

For simple $m\text{BH}_n$ radicals, $m = 2$ in our cases, on the $\text{Si}\{001\}3 \times 1:\text{H}$ surfaces, the structural optimizations showed strong relaxation and structural reconstructions. As a

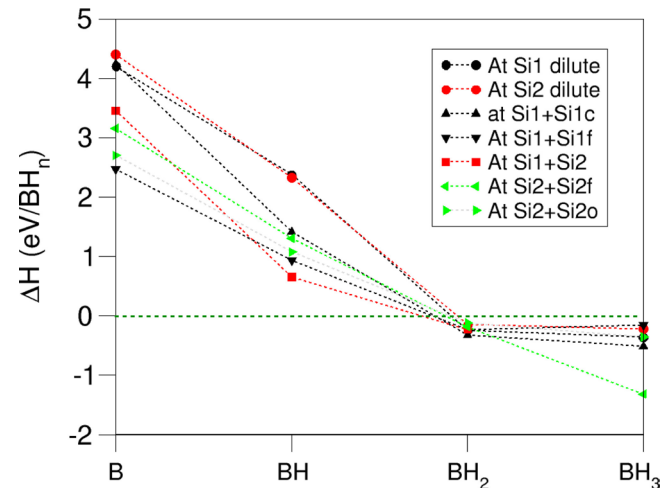


Figure 7. The calculated formation enthalpies the deposited BH_n radicals on the $\text{Si}\{001\}3 \times 1:\text{H}$ surface with different configurations according to equations (2)–(5). The dotted lines are used to guide the readers' eyes.

consequence, most of the configurations contain defect states at the forbidden gaps as shown in figure 6 and in table SM-2. These defect states are position deeper in energy in the forbidden gap than those of the isolated BH_n on the surface. This trend implies that further deposition of boron/boranes on the silicon surface will induce more defects and finally form a Si/B interface.

3.5. Summary of the energetics of BH_n on $\text{Si}\{001\}3 \times 1:\text{H}$ surface

Here we summarize the formation enthalpies, chemical bonding, and charge/charge transfer from the first-principles calculations. Figure 7 shows the dependences of formation enthalpies on the number of H in BH_n radicals.

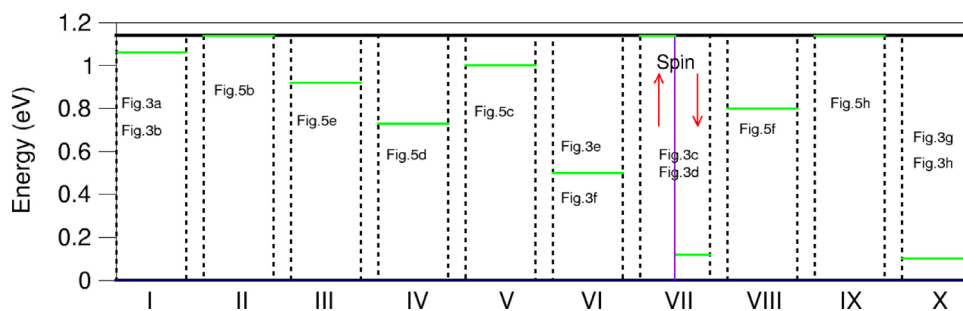


Figure 8. Schematic electronic structures of the configurations of high stability based on our electronic structure calculations. The dark solid line (upper) represents for the bottom of the conduction band of $\text{Si}(001)3 \times 1\text{:H}$; the blue line (bottom) for the top of the valence band (Fermi level); the dotted lines are used to separate the Cases. The green short lines represent the defect states. The electronic properties of the BH_n deposited $\text{Si}\{001\}3 \times 1\text{:H}$ surfaces are classified into the cases.

Clearly, the formation enthalpies decrease with increasing n in BH_n radicals. For dilute cases, the formation enthalpies are positive when a B or BH deposited on Si1 and Si2, respectively. The formation enthalpies become negative when a BH_2 or a BH_3 deposits on the surface Si. That means that energetically, deposition of BH_3 on the surface Si or the reaction is favored.

Based on the electronic structure calculations, we summarize the electronic properties of the investigated configurations of high stability in figure 8.

Deposition of borane on the $\text{Si}\{001\}3 \times 1\text{:H}$ surface results a rich variety of electronic properties depending on the deposition molecules and the sites. Deposition of a BH_2 on either the Si1 or the Si2 site produces a shallow hole below the conduction band (Case I). When two BH_2 radicals were deposited on two Si1 sites which are not close to each other, the obtained system has the defect states similar to that of case II. Meanwhile, when two BH_2 radicals were deposited on one Si1–Si1 chain, structural relaxation occurs, which causes the disappearing of the defect states from the forbidden gap (Case II). As shown in cases III, IV and V, depositing two BH_2 at different sites induces defect states in the gap. Notably exchange a B in the BH_2 and the nearby Si causes a defect state at the middle of the energy gap (Case VI).

When an isolated BH_3 molecule is deposited on a Si site of the Si surface, the system becomes spin-polarized. This is due to the unpaired electron from the BH_3 radical (Case VII). The defect state for the spin-down electrons is about 01 eV above the Fermi level. The band for the spin-up electrons remain a semiconducting, whereas the band for the spin-down electrons becomes metallic. The exchange of B in the BH_3 molecule and the nearby Si keeps the defect state at the same energy but the spin-polarization disappears (Case X). Deposition of two BH_3 molecules at different sites induces defect states in the band gap (Case VIII and IX).

Overall the band structure calculations demonstrated a rich variety of defect states in the forbidden gap of Si. This also means that a rigid electron counting model can not be used to

predict the electronic properties of the products prepared at the early stage of PureB process.

4. Conclusions

First, AIMD simulations for BH_3 molecules on $\text{Si}\{001\}3 \times 1\text{:H}$ surfaces at about 673 K have revealed the atomistic details of deposition of BH_3 and the correspondingly formation of $-\text{SiBH}_4$ radicals on the surfaces. The MD simulations showed the decomposition of $-\text{SiBH}_4$ via the surface reaction $-\text{SiBH}_4 \rightarrow -\text{SiBH}_2 + \text{H}_2(\text{g})$. The present study also revealed the importance of the van der Waals correction to the standard DFT functional in description of molecular/surface interactions. Secondly, total energy calculations showed high stability of the formed $-\text{SiBH}_2$ and $-\text{SiBH}_3$ radicals at the *initial* stage which is similar to the case of BH_n radicals depositing on the high temperature $\text{Si}\{001\}2 \times 1\text{:H}$ surface. However, the $\text{Si}\{001\}3 \times 1\text{:H}$ surfaces provides more deposition sites, which results a richer variety of local structures and electronic properties. The high stability of B/Si exchanged systems with $(-\text{B})-\text{SiH}_n$ ($n = 1$ to 3) configurations indicates possibilities of B existing at and diffusing into the Si surface. Thirdly, calculations showed that $m\text{BH}_n$ clustering (the simple cases $m = 2$) can cause structural reconstructions. The reconstructed structures, especially the formation of B–B bond significantly stabilize the deposited systems. These results indicate further reactions for thicker BH_n depositions, which deserves further investigation. Finally, the electronic structure calculations showed that surface structural relaxation and reconstructions have significant impacts on the electronic properties. There are different defect states in the energy gaps, depending on the deposited radicals and local bonding. The currently used electron counting model is violated in many cases. These defect states largely determine the electronic and optical properties of the deposited surfaces. The defect states obtained here provide an explanation for the experimental observations of dramatic changes of the electrical conductivity and optical properties with very thin atomic layer deposition

of BH_n radicals. These insights can aid development of new PureB processes for new heterojunctions for detection of UV photons.

Acknowledgments

We thank Mr Lele Fang (Radboud University Nijmegen) for useful discussions and for reading the manuscript.

Supplementary materials

The supplementary materials associated with this article can be found in the online version.

Conflicts of interest

There are no conflicts to declare.

ORCID iDs

C M Fang  <https://orcid.org/0000-0003-0915-7453>

M H F Sluiter  <https://orcid.org/0000-0002-6514-4318>

References

- [1] Sarubbi F, Nanver L K and Scholters L M 2010 *IEEE Trans. Electron Devices* **57** 1260
- [2] Shi L, Sarubbi F, Naver L K, Kroth U, Gottwald A and Nihtianov S 2010 *Procedia Eng.* **5** 633
- [3] Mohammadi V, de Boer W B and Naver L K 2012 *Appl. Phys. Lett.* **101** 111906
- [4] Mohammadi V, de Boer W B and Naver L K 2012 *J. Appl. Phys.* **112** 113501
- [5] Mohammadi V, de Boer W B, Scholtes T L M and Naver L K 2013 *ECS Trans.* **45** 57
- [6] Sarubbi F, Nanver L K and Scholters T L 2006 *ECS Trans.* **3** 35
- [7] Mohammadi V, Rao P R, van de Kruijs R W E and Nihtianov S 2015 *73rd Annual Device Research Conf. (DRC)* pp 73–4
- [8] Mohammadi V, Nihtianov S and Fang C M 2017 *Sci. Rep.* **7** 13247
- [9] Bragg J K, McCarty L V and Norton F J 1951 *J. Am. Chem. Soc.* **73** 2134
- [10] Bauer S H 1958 *J. Am. Chem. Soc.* **80** 294
- [11] Fehlner T P 1965 *J. Am. Chem. Soc.* **87** 4200
- [12] Habuka H, Akiyama S, Otsuka T and Qu W F 2000 *J. Cryst. Growth* **209** 807
- [13] Hannon J B, Hibino H, Bartelt N C, Swartzentruber B S, Ogino T and Kellogg G L 2000 *Nature* **405** 552
- [14] Ramstad A, Brocks G and Kelly P J 1995 *Phys. Rev. B* **51** 14504
- [15] Perrine K A and Tepliyakov A V 2010 *Chem. Soc. Rev.* **39** 3256
- [16] Hakala M, Puska M J and Nieminen R M 2000 *Phys. Rev. B* **61** 8155
- [17] Pi X D, Chen X B and Yang D R 2011 *J. Phys. Chem. C* **115** 9838
- [18] Zavodinsky V G, Chukurov E N and Kuyanov I A 2009 *Surf. Rev. Lett.* **16** 167
- [19] Boukari K, Sonnet P and Duverger E 2012 *Chem. Phys. Chem.* **13** 3945
- [20] Shayeganfar F and Rochefort A 2015 *J. Phys. Chem. C* **119** 15742
- [21] Hu S W, Wang Y and Wang X Y 2003 *J. Phys. Chem. A* **107** 1635
- [22] Fang C M, Mohammadi V, Nihtianov S and Sluiter M H F 2017 *Comput. Mater. Sci.* **140** 253
- [23] Wyckoff R W G 1963 *Crystal Structures* (New York: Wiley)
- [24] Hohenberg P and Kohn W 1964 *Phys. Rev. B* **136** 864
- [25] Kohn W and Sham L J 1965 *Phys. Rev. A* **140** 1133
- [26] Kresse G and Hafner J 1994 *Phys. Rev. B* **49** 14251
- [27] Kresse G and Furthmüller J 1995 *J. Comput. Mater. Sci.* **6** 15
- [28] Blöchl P E 1994 *Phys. Rev. B* **50** 17953
- [29] Kresse G and Joubert J 1999 *Phys. Rev. B* **59** 1758
- [30] Perdew J P, Burke K and Ernzerhof M 1996 *Phys. Rev. Lett.* **77** 3865
- [31] Monkhorst H J and Pack J D 1976 *Phys. Rev. B* **13** 5188
- [32] Huber K P and Herzberg G 1979 *Molecular Spectra and Molecular Structure. IV. Constants of Diatomic Molecules* (New York: Van Nostrand Reinhold Co)
- [33] Lide D R 2003 *CRC Handbook of Chemistry and Physics* 84th edn (Boca Raton, FL: CRC Press)
- [34] Jones R O 2015 *Rev. Mod. Phys.* **87** 897
- [35] Bader R F W and Beddal P M 1971 *Chem. Phys. Lett.* **8** 29
- [36] Bader R F W, Nguyen T T and Tal Y 1981 *Prog. Phys.* **44** 893
- [37] Bader R F 1998 *J. Phys. Chem. A* **102** 7314
- [38] Dion M, Rydberg H, Schröder E, Langreth D C and Lundqvist B I 2004 *Phys. Rev. Lett.* **92** 246401
- [39] Klimeš J, Bowler D R and Michaelides A 2011 *Phys. Rev. B* **83** 195131
- [40] Fang C M, Li W-F, Koster R, Klimeš J, van Blaaderen A and van Huis M A 2015 *Phys. Chem. Chem. Phys.* **17** 365